SCIENTIFIC REPORTS

OPEN

SUBJECT AREAS:
NANOTECHNOLOGY
APPLIED PHYSICS
OPTICAL MATERIALS AND STRUCTURES
SURFACE PATTERNING AND IMAGING

Received
15 September 2011

Accepted
11 November 2011

Published
29 November 2011

Correspondence and requests for materials should be addressed to X.Z. (xiang@berkeley.edu)

* These authors contributed equally to this work.

Maskless Plasmonic Lithography at 22 nm Resolution

Liang Pan[1]*, Yongshik Park[1]*, Yi Xiong[1]*, Erick Ulin-Avila[1], Yuan Wang[1], Li Zeng[1], Shaomin Xiong[1], Junsuk Rho[1], Cheng Sun[2], David B. Bogy[1] & Xiang Zhang[1]

[1]Department of Mechanical Engineering, University of California, Berkeley, CA 94720-1740, USA, [2]Department of Mechanical Engineering, Northwestern University, Evanston, IL 60208-3111, USA.

Optical imaging and photolithography promise broad applications in nano-electronics, metrologies, and single-molecule biology. Light diffraction however sets a fundamental limit on optical resolution, and it poses a critical challenge to the down-scaling of nano-scale manufacturing. Surface plasmons have been used to circumvent the diffraction limit as they have shorter wavelengths. However, this approach has a trade-off between resolution and energy efficiency that arises from the substantial momentum mismatch. Here we report a novel multi-stage scheme that is capable of efficiently compressing the optical energy at deep sub-wavelength scales through the progressive coupling of propagating surface plasmons (PSPs) and localized surface plasmons (LSPs). Combining this with airbearing surface technology, we demonstrate a plasmonic lithography with 22 nm half-pitch resolution at scanning speeds up to 10 m/s. This low-cost scheme has the potential of higher throughput than current photolithography, and it opens a new approach towards the next generation semiconductor manufacturing.

Creating super-fine nano-scale patterns with high throughput is essential for high-speed computing, data storage and broader applications for nano-manufacturing. Photolithography has been the most successful process for continuing the scaling down of semiconductor devices as predicted by Moore's law[1,2]. However, due to the diffractive nature of light, it becomes increasingly costly and difficult for the current optical lithography to continue the reduction of node size. For example, the state-of-the-art optical immersion tool cost for dedicated double- and multiple- patterning techniques is exceeding $50 M per tool. And the process complexity now makes the mask set cost over 5 million US dollars because of the large amount of data required to write these masks and the difficulties in implementing the necessary optical proximity correction[3]. Because of the ever-increasing complexity and cost of the mask-based lithography, maskless schemes are emerging as a viable approach by eliminating the need for masks to reduce cost and design cycle[4]. However, the low throughput of most maskless methods due to the serial and slow scanning nature remains the bottleneck. Although multi-axial electron-beam lithography has been proposed to increase throughput by using multiple beams in a parallel manner, there are difficulties in simultaneously regulating the multiple beam sizes and positions because of the thermal drift and electrical charge Coulomb interactions, which result in significant lens aberration[5–11]. Another optical maskless approach is to use assisting light beams to control the resist kinetics to achieve subdiffraction features[12–14]. It provides a low-cost alternative, however the achievable feature size is still greatly affected by the spatial regulation capability of the far field optics. A major improvement in maskless lithography is thus critical in order to satisfy the demands in mass production for the semiconductor industry. Working at optical near-field is another approach to overcome the resolution limitation of conventional photolithography techniques, but it still faces key obstacles such as energy throughput and working distance control for high volume manufacturing[15–21]. To overcome those limitations, the plasmonic nanolithography (PNL) technique has been explored for high-speed maskless nearfield nano-patterning using a plasmonic lens (PL)[22]. Despite the promising potential of PNL, important issues such as the trade-off between spatial confinement and inherit loss of surface plasmons (SPs), and therefore the throughput, are yet to be solved before this approach becomes practically viable. A fundamentally new optical scheme in realizing efficient optical confinement at deep sub-wavelength scale is needed.

PSP and LSP have been used in high resolution optical imaging, light delivery and lithography beyond the diffraction limit[18,21,23–41]. Typical PSP is suitable for optical wave guiding applications, however, its poor spatial confinement makes it difficult to further scale-down the resolution[42–46]. On the other hand, LSP can achieve deep sub-wavelength optical confinement, but it does not provide enough energy throughput due to its resonating nature that causes strong losses. Through adiabatic transformation, it has been proposed to convert the PSP

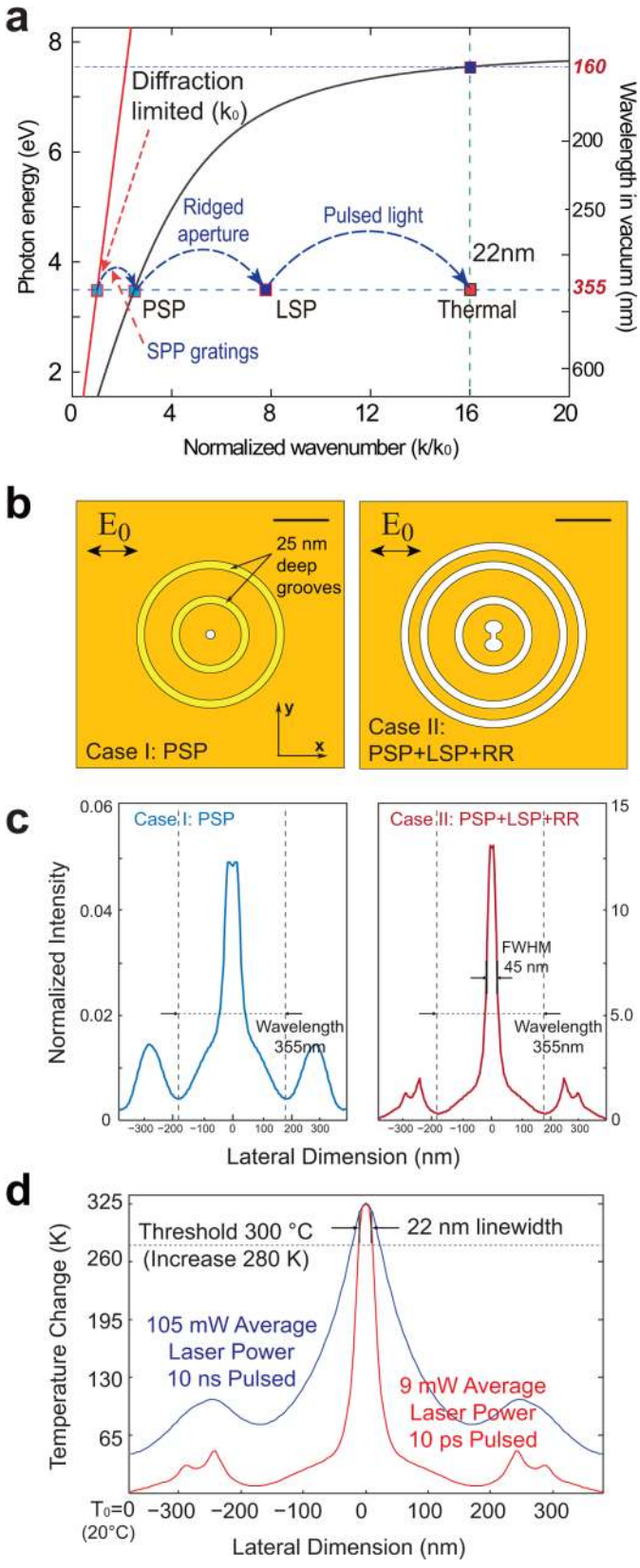

Figure 1 | Progressive multi-stage focusing scheme efficiently squeezes light to the deep sub-wavelength scale. (a) The accessible wavenumber range (red line) for conventional optics is limited to k_0 by diffraction. The dispersive nature of the propagating surface plasmon (PSP) allows accessing a broader range of wavenumbers (black solid line), however a very short excitation wavelength (160 nm) is still required to resolve 22 nm features with high intrinsic loss. Our multi-stage approach allows accessing the same features at 1/16 of the excitation wavelength through a progressive multi-stage focusing scheme. (b) Designs of plasmonic lens (PL) structures and simulation results. Two cases of PL designs are shown here for comparison, including: case I (left), a PL consisting of two ring grooves and a centered 40-nm diameter circular aperture working with PSP; case II (right), a multi-stage plasmonic lens (MPL) consisting of two ring grating slits with the dumbbell-shaped aperture and an additional outer ring reflector (RR) slit working with both PSP and localized surface plasmon (LSP). Both of them are made of a 60-nm Cr thin film and optimized for illumination at 355 nm wavelength with linear polarization along the x-axis. Both scale bars are 500 nm. (c) The simulated light intensity profiles at the plane 10 nm away from the lens along the x-axis which are normalized to the incident light. At the deep sub-wavelength region, the PSP itself is incapable of sustaining high transmission through the circular aperture, but the LSP greatly helps to improve the center transmission by several orders. (d) Temperature profiles in the thermal type resist layer under MPL heating. Two different time durations of laser pulse of 10 ps (red) and 10 ns (blue), respectively, have been used in the numerical study. By properly controlling the laser power level and pulse duration, we can further improve the feature size down to 22 nm. The ps-pulsed laser has great advantages over the modulated continuous-wave laser in terms of pattern size and contrast.

modes efficiently for imaging, sensing, energy conversion and storage[43,47–50]. Here we report a new nano- focusing scheme based on a multi-stage plasmonic lens (MPL) design on an air bearing surface (ABS) utilizing both PSP and LSP. Through this progressive focusing scheme, as illustrated in Fig. 1a, that combines PSP focusing, LSP conversion and nano-scale thermal management on the photoresist, we are able to efficiently squeeze light into the deep sub-wavelength scale and achieve nanolithography with 22 nm resolution using a 355 nm pulsed laser source. In comparison with the state-of-art immersion photolithography, our plasmonic lithography system costs orders of magnitude less than the current lithography tool.

Results

The key MPL design to achieve the high resolution with the required throughput consists of a dumbbell-shaped aperture, a set of ring couplers (two inner rings) and a ring reflector (the outer ring), fabricated on a metallic thin film. As schematically illustrated in Fig. 1a, the PSPs are excited and propagate towards the center of MPL by using a circular shape grating, where they are further efficiently converted into deep subwavelength LSPs through the dumbbell-shaped aperture, thereby achieving an optical confinement of less than 50 nanometers. In comparison to the extremely low optical transmission through the deep-subwavelength holes, a MPL can provide 5∼10 orders of magnitude higher optical transmission in the same area which ensures that the focused light spot has enough energy for writing patterns at an extremely fast scanning speed[51,52].

Through electromagnetic simulation we compared two plasmonic structure designs working at the excitation wavelength of 355 nm with their corresponding light intensity normalized by the incident light intensity (CST Microwave Studio). In Figure 1b, case I shows an example of PSP-based PL with a 40 nm diameter circular aperture at its center[17,27]. By guiding the PSP energy towards the center it is capable of producing orders of magnitude higher transmission through the same size hole. However, it can be seen that the net transmission through a PSP-based PL decreases rapidly when the center hole size further reduces into the deep sub-wavelength region. Case II shows our new MPL design where the center hole is replaced by a dumbbell-shaped aperture in order to convert PSP into LSP to enhance the confinement and intensity at the focal point[53–56]. The performance of the MPL is further improved by adding a third ring placed at a half-wave length position of the circular grating so that it acts as a reflector for the outward propagating PSP waves due to deconstructive interference. The central focal spot by the MPL has

a peak intensity of 13.1 times the incidence light with a 45 nm FWHM spot size. The ring gratings are etched all the way through the metal film thereby causing the side lobes with a maximum intensity of 2.0 times of incidence, corresponding to a contrast ratio of 6.5 to the focal spot intensity, which is well under the exposure threshold for our current maskless lithography purpose. The contrast ratio can be further enhanced to 70 or more by replacing the grating slits with shallow blind grooves similar as those used in case I (shown in supporting online material (SOM)). High throughput writing requires using a large number of lens array at high speed, which calls for efficient PSP energy utilization for each lens. We designed the MPL with a diameter of about 1 μm with a Cr metal layer because its superb mechanical properties can prevent lens damage when the lens flies within a few nanometers above the substrate at high speeds of several meters per second. Replacing Cr with other metals, such as aluminum with a better mechanical lens protection can further improve the peak intensity by a few times (see in SOM).

Instead of continuous-wave laser we use a pulsed laser with a thermal resist to achieve the high resolution and patterning throughput by lowering the required operating laser power level and controlling the heat diffusion at the nano-scale. Figure 1d shows the simulated temperature profiles in the thermal resist layer under heating from the optical field of focused plasmons from MPL under two different laser pulses. With 10 ps-pulses, we can further improve the feature size down to 22 nm (about half of the optical spot of 45 nm focused by the MPL) and reduce the required laser average power from 105 mW to merely 9 mW by utilizing the nonlinear and time dependent response of thermal resist[57,58]. The high-speed plasmonic writing involves the competition of optical absorption at the nano-scale, heat accumulation and thermal diffusion. The energy deposited into the nano-scale resist volume can rapidly diffuse into the neighboring region within a nanosecond, which enlarges the exposed features, increases the required laser power, and causes pattern distortion. Therefore, the pulsed laser has great advantages over the continuous-wave laser for ensuring the good thermal confinement in the resist layer. Application of the pulsed laser also allows the employment of a PL array for parallel patterning.

Using advanced ABS techniques, we can fly a scanning device of a few millimeters that carries arrays of MPLs (up to 16,000) at sub-10 nm above a resist surface with a speed of 4∼14 m/s (Figure 2). We experimentally demonstrated high throughput direct writing at 22-nm half pitch and the parallel patterning. The ABS technique used for the scanning gap control is a self-positioning method which can maintain a consistent nano-scale gap during high speed scanning. The air flow created by the relative motion between the rotating substrate and the ABS generates an aerodynamic lift force, which is balanced by the force supplied by a spring suspension. Due to the high air bearing stiffness and small actuation mass, the flying head can follow the substrate profile and maintain a consistent flying height of 5–20 nm with sub 1-nm variation. The ABS was designed

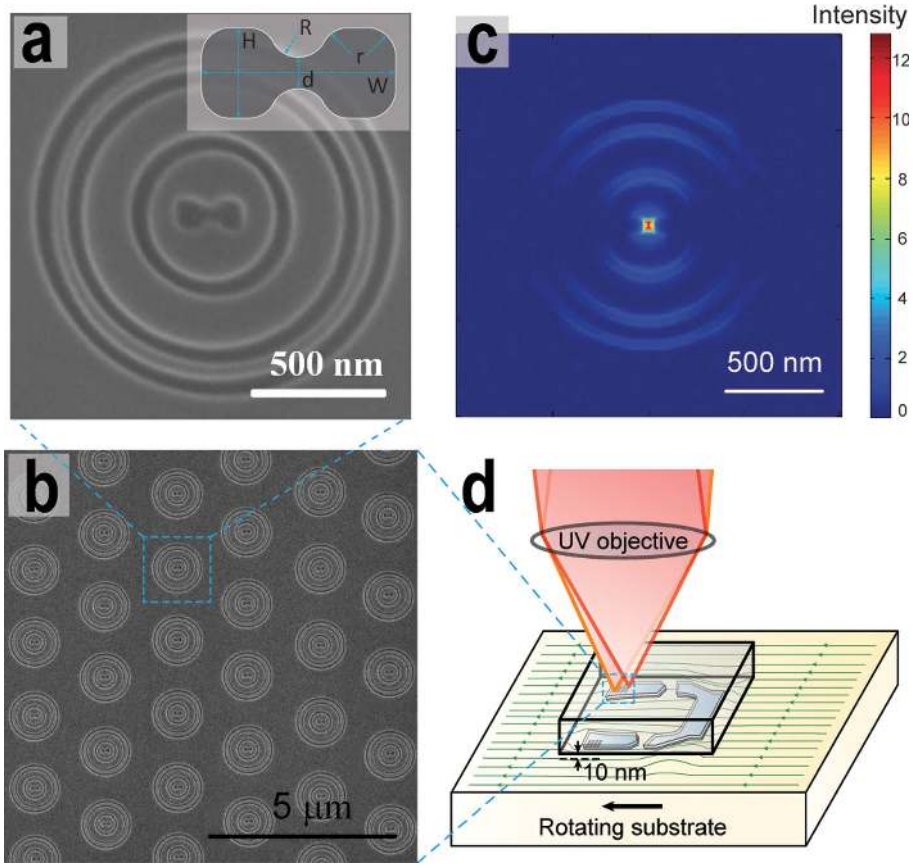

Figure 2 | MPL array and plasmonic flying head enable high-throughput maskless plasmonic nanolithography (PNL) by focusing the ultraviolet laser energy into nano-scale spots onto the high speed spinning substrate. (a) The SEM picture of a multistage plasmonic lens (MPL) consisting of a dumbbell-shaped aperture, a set of ring couplers (two inner rings) and a ring reflector (the outer ring), fabricated on a metallic thin film in 60 nm thick Cr film. The parameters of the centre aperture are shown in the insert, where W=240 nm, H=98 nm, R=35 nm, r=40 nm, and d=26 nm. The radii of the three rings are 240 nm 480 nm, and 600 nm, respectively. And the width of the rings is 50 nm. (b) A SEM image of hexagonally packed MPL array. (c) The field intensity distribution at the plane 10 nm distance away from the MPL surface normalized to the incident intensity of 355 nm wavelength light. The half-circular shaped side lopes in the intensity profile are the direct transmissions through the three rings and their intensities are far below the exposure threshold of the resist. (d) A plasmonic flying head uses advanced airbearing surface (ABS) technology to maintain the gap between the lenses and the substrate at 10 nm at a linear scanning speed of 10 m/s.

using an in-house developed air bearing simulators[59] and fabricated at the bottom of the transparent flying head made of sapphire using micro-fabrication. With careful ABS design, it is possible to achieve a consistent working gap at a wide range of substrate rotation speeds and radial positions, and therefore eliminate the need for a high bandwidth feedback control loop, one of the major technical barriers for high speed patterning using AFM-type scanning probes. In our work, the working gap is 10 nm over the velocity range from 4 to 14 m/s with a sub-1 nm variation. The pitch and roll angles of the flying head are kept consistent at 40 μrad and sub-1 μrad, respectively. The array of MPL (SEM image shown in Fig. 2a, b) was later fabricated by focused ion beam milling on a 60-nm thick chromium (Cr) thin film coated on the ABS. Figure 2c shows the field intensity distribution at the plane 10 nm distance away from the lens and has been normalized to the incident light intensity. As schematically shown in Fig. 2d, each of the MPLs can be controlled using independent laser beam in order to enable high-throughput parallel writing.

Figures 3a, b show the AFM image of closely patterned dots with 22 nm half pitch resolution by PNL with the cross-sectional scan (Fig. 3c). The results are in agreement with the experimental conditions (substrate velocity at 7 m/s and the laser pulse repetition rate at 160 MHz), and each dot is generated by a single laser pulse. Similar to other maskless approaches, writing at a higher laser power or higher pattern spatial frequency allows the dots to merge into continuous lines with different widths. The result is shown in Figure 4 where two MPLs in the lens array independently write on the thermal resist in parallel. To obtain 50-nm wide solid lines, the MPL1 was excited with a laser power twice that used for Figure 3, and the MPL2 simultaneously used a ramping laser power varying from 2 to 4 times. It is shown that the exposure feature size can be controlled by regulating the laser power during the pattern writing. It should also be noted that the pattern definition can be greatly improved by the optimization of the resist exposure threshold and post-development conditions.

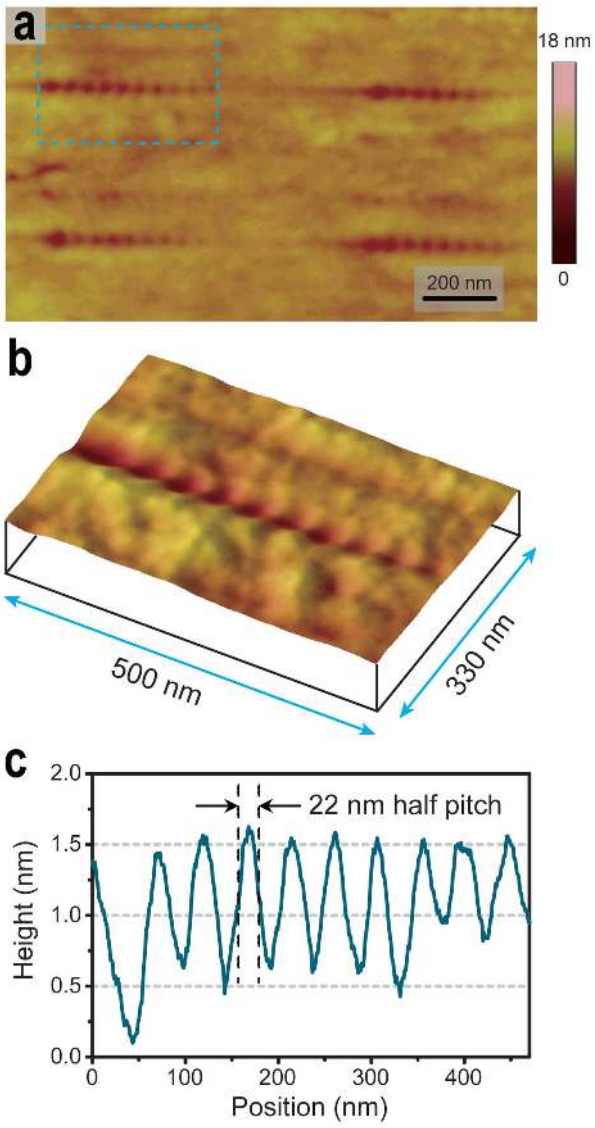

Figure 3 | AFM image of closely packed dots at 22-nm half pitch on the thermal resist. (a) the AFM image of four trains of dot lines, (b) the 3D topography of the boxed dot line in Figure a, and (c) the cross-sectional profile of the dot line in Figure b.

Discussion

In summary, we have demonstrated a high speed plasmonic nanolithography with 22 nm half-pitch resolution. This is achieved by employing multi-stage plasmon focusing through relatively low-loss propagating surface plasmons focusing and later conversion to localized plasmons. This allows the highly efficient transmission and focusing of near-field spot which is the key to improving the throughput, for a given laser power, by increasing the scanning speed and/or by employing a great number of MPLs and flying heads for parallel patterning. In principle, this scheme allows a single flying head to carry up to 16,000 MPLs, which can pattern a 12-inch wafer in minutes. This is comparable to conventional production-level photolithography but at a much higher resolution of 22 nm half-pitch size. This new scheme enables a low cost, high-throughput maskless nano-scale fabrication with a few orders of magnitude higher throughput than conventional maskless approaches. It may allow continuously scaling to smaller node size beyond 22 nm by utilizing shorter SPs wavelength and guiding mechanisms, and it opens up a promising route towards the next generation lithography for semiconductor manufacturing[47]. In addition, it also holds a great potential in the next generation magnetic data storage, known as heat assisted magnetic recording (HAMR) and Bit-Patterned Media (BPM), to achieve two orders higher capacities in the future[60].

Methods

In the nanolithography experiments (detailed system layout is shown in SOM), a spindle was used to rotate the substrate with the resist at 2,500 rpm corresponding to a linear speed of 4~14 m/s at different radii, and a picosecond pulsed UV laser (Vanguard, Spectra-Physics, 355 nm wavelength) was used as the exposure light. Through a single UV objective, a few individually modulated laser pulse trains were first focused down to separated spots with diameter of several micrometers to

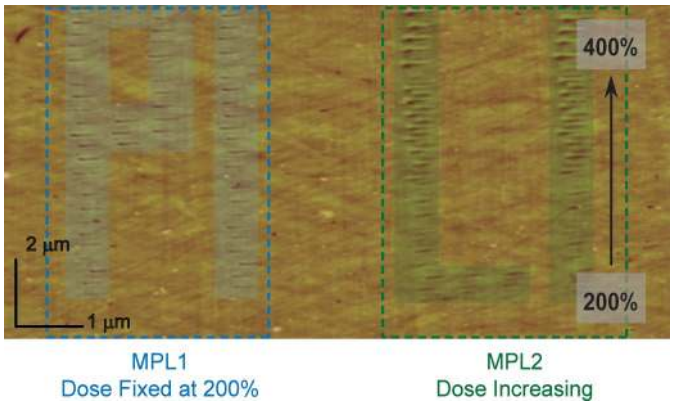

Figure 4 | AFM image of a PNL parallel writing result on the thermal resist. Two of MPLs in an array were used to simultaneously write independent patterns, capital letters "PI" and "LI", respectively. MPL1 used a fixed laser power at 2 times that used in generating the result in Fig. 3, and MPL2 used an increasing power varying from 2 to 4 times. As the laser power level further increases, the side lobe patterns from the MPL start to show on the resist layer.

illuminate the area of the designated MPL structure on the ABS surface (at the bottom of the flying head). Then, each of the MPLs further focuses the pre-focused light spot to a nano-scale spot for patterning the resist layer. The information of the relative position between the flying head and substrate is provided by the spindle encoder (angular) and a linear nano-stage (radial), which feeds to a home-made pattern generator to pick the laser pulse for exposure through an optical modulator. During the test, an interferometry setup and an acoustic emission sensing module were installed to monitor the real-time motion of the flying head during the lithography process. The resist used in our test is $(TeO_2)_xTe_yPd_z$ [x≈80% wt., y≈10% wt., z≈10% wt.], an inorganic thermal type developed on the basis of the Te-TeO_x resist. Pd is added to the Te-TeO_x in order to enhance the exposure uniformities and resist resolution by forming finer crystalline grains during phase transition, and its thermal stability is also beneficially improved. This inorganic resist is employed also because of its good mechanical properties for tribological concerns, and good sensitivity for high-resolution. After the PNL experiment, the exposed patterns were developed in diluted KOH solution and then examined by an atomic force microscope (AFM).

1. Jeong, H. J. *et al.* The future of optical lithography. *Solid State Technol.* **37**, 39–47 (1994).
2. Okazaki, S. Resolution limits of optical lithography. *J. Vac. Sci. Technol. B* **9**, 2829–2833 (1991).
3. Hughes, G., Litt, L. C., Wüest, A. & Palaiyanur, S. Mask and wafer cost of ownership (COO) from 65 to 22 nm half-pitch nodes. *Proc. SPIE* **7028** (2008).
4. International technology roadmap for semiconductors 2009 edition: Lithography. (2009).
5. Melngailis, J. Focused ion-beam technology and applications. *J. Vac. Sci. Technol. B* **5**, 469–495 (1987).
6. Chao, D., Patel, A., Barwicz, T., Smith, H. I. & Menon, R. Immersion zone-plate-array lithography. *J. Vac. Sci. Technol. B* **23**, 2657–2661 (2005).
7. Piner, R. D., Zhu, J., Xu, F., Hong, S. H. & Mirkin, C. A. "Dip-pen" nanolithography. *Science* **283**, 661–663 (1999).
8. Groves, T. R. & Kendall, R. A. Distributed, multiple variable shaped electron beam column for high throughput maskless lithography. *J. Vac. Sci. Technol. B* **16**, 3168–3173 (1998).
9. Muraki, M. & Gotoh, S. New concept for high-throughput multielectron beam direct write system. *J. Vac. Sci. Technol. B* **18**, 3061–3066 (2000).
10. Salaita, K. *et al.* Massively parallel dip-pen nanolithography with 55000-pen two-dimensional arrays. *Angew. Chem.-Int. Edit.* **45**, 7220–7223 (2006).
11. Vettiger, P. *et al.* The "Millipede" - More than one thousand tips for future AFM data storage. *IBM J. Res. Dev.* **44**, 323–340 (2000).
12. Scott, T. F., Kowalski, B. A., Sullivan, A. C., Bowman, C. N. & McLeod, R. R. Two-Color Single-Photon Photoinitiation and Photoinhibition for Subdiffraction Photolithography. *Science* **324**, 913–917 (2009).
13. Li, L., Gattass, R. R., Gershgoren, E., Hwang, H. & Fourkas, J. T. Achieving λ/20 Resolution by One-Color Initiation and Deactivation of Polymerization. *Science* **324**, 910–913 (2009).
14. Andrew, T. L., Tsai, H.-Y. & Menon, R. Confining Light to Deep Subwavelength Dimensions to Enable Optical Nanopatterning. *Science* **324**, 917–921 (2009).
15. Srisungsitthisunti, P., Ersoy, O. K. & Xu, X. F. Improving near-field confinement of a bowtie aperture using surface plasmon polaritons. *Appl. Phys. Lett.* **98**, 223106 (2011).
16. Tominaga, J., Nakano, T. & Atoda, N. An approach for recording and readout beyond the diffraction limit with an Sb thin film. *Appl. Phys. Lett.* **73**, 2078–2080 (1998).
17. Lezec, H. J. *et al.* Beaming light from a subwavelength aperture. *Science* **297**, 820–822 (2002).
18. Liu, Z., Lee, H., Xiong, Y., Sun, C. & Zhang, X. Far-field optical hyperlens magnifying sub-diffraction-limited objects. *Science* **315**, 1686–1686 (2007).
19. Vedantam, S. *et al.* A plasmonic dimple lens for nanoscale focusing of light. *Nano Lett.* **9**, 3447–3452 (2009).
20. Ozbay, E. Plasmonics: Merging photonics and electronics at nanoscale dimensions. *Science* **311**, 189–193 (2006).
21. Fang, N., Lee, H., Sun, C. & Zhang, X. Sub-diffraction-limited optical imaging with a silver superlens. *Science* **308**, 534–537 (2005).
22. Srituravanich, W. *et al.* Flying plasmonic lens in the near field for high-speed nanolithography. *Nat. Nanotechnol.* **3**, 733–737 (2008).
23. Sundaramurthy, A. *et al.* Toward nanometer-scale optical photolithography: Utilizing the near-field of bowtie optical nanoantennas. *Nano Lett.* **6**, 355–360 (2006).
24. Challener, W. A. *et al.* Heat-assisted magnetic recording by a near-field transducer with efficient optical energy transfer. *Nat. Photonics* **3**, 220–224 (2009).
25. Ebbesen, T. W., Lezec, H. J., Ghaemi, H. F., Thio, T. & Wolff, P. A. Extraordinary optical transmission through sub-wavelength hole arrays. *Nature* **391**, 667–669 (1998).
26. Barnes, W. L., Dereux, A. & Ebbesen, T. W. Surface plasmon subwavelength optics. *Nature* **424**, 824–830 (2003).
27. Srituravanich, W., Fang, N., Sun, C., Luo, Q. & Zhang, X. Plasmonic nanolithography. *Nano Lett.* **4**, 1085–1088 (2004).
28. Grosjean, T., Mivelle, M., Baida, F. I., Burr, G. W. & Fischer, U. C. Diabolo nanoantenna for enhancing and confining the magnetic optical field. *Nano Lett.* **11**, 1009–1013 (2011).
29. Lindquist, N. C., Nagpal, P., Lesuffleur, A., Norris, D. J. & Oh, S. H. Three-dimensional plasmonic nanofocusing. *Nano Lett.* **10**, 1369–1373 (2010).
30. Liu, Y. M., Zentgraf, T., Bartal, G. & Zhang, X. Transformational plasmon optics. *Nano Lett.* **10**, 1991–1997 (2010).
31. Ropers, C. *et al.* Grating-coupling of surface plasmons onto metallic tips: A nanoconfined light source. *Nano Lett.* **7**, 2784–2788 (2007).
32. Sondergaard, T. *et al.* Resonant plasmon nanofocusing by closed tapered gaps. *Nano Lett.* **10**, 291–295 (2010).
33. Volkov, V. S. *et al.* Nanofocusing with channel plasmon polaritons. *Nano Lett.* **9**, 1278–1282 (2009).
34. Liu, N., Tang, M. L., Hentschel, M., Giessen, H. & Alivisatos, A. P. Nanoantenna-enhanced gas sensing in a single tailored nanofocus. *Nat Mater* **10**, 631–636 (2011).
35. Kim, S. *et al.* High-harmonic generation by resonant plasmon field enhancement. *Nature* **453**, 757–760 (2008).
36. Zentgraf, T., Liu, Y. M., Mikkelsen, M. H., Valentine, J. & Zhang, X. Plasmonic Luneburg and Eaton lenses. *Nat. Nanotechnol.* **6**, 151–155 (2011).
37. Kinkhabwala, A. *et al.* Large single-molecule fluorescence enhancements produced by a bowtie nanoantenna. *Nat. Photonics* **3**, 654–657 (2009).
38. Radko, I. P., Bozhevolnyi, S. I., Evlyukhin, A. B. & Boltasseva, A. Surface plasmon polariton beam focusing with parabolic nanoparticle chains. *Opt. Express* **15**, 6576–6582 (2007).
39. Bozhevolnyi, S. I. & Nerkararyan, K. V. Adiabatic nanofocusing of channel plasmon polaritons. *Opt. Lett.* **35**, 541–543 (2010).
40. Davoyan, A. R., Shadrivov, I. V., Zharov, A. A., Gramotnev, D. K. & Kivshar, Y. S. Nonlinear Nanofocusing in Tapered Plasmonic Waveguides. *Phys. Rev. Lett.* **105**, 116804 (2010).
41. Wang, Y., Srituravanich, W., Sun, C. & Zhang, X. Plasmonic nearfield scanning probe with high transmission. *Nano Lett.* **8**, 3041–3045 (2008).
42. Anker, J. N. *et al.* Biosensing with plasmonic nanosensors. *Nat. Mater.* **7**, 442–453 (2008).
43. Dionne, J. A., Sweatlock, L. A., Atwater, H. A. & Polman, A. Plasmon slot waveguides: Towards chip-scale propagation with subwavelength-scale localization. *Phys. Rev. B* **73**, 035407 (2006).
44. Oulton, R. F., Sorger, V. J., Genov, D. A., Pile, D. F. P. & Zhang, X. A hybrid plasmonic waveguide for subwavelength confinement and long-range propagation. *Nat. Photonics* **2**, 496–500 (2008).
45. Maier, S. A. *et al.* Local detection of electromagnetic energy transport below the diffraction limit in metal nanoparticle plasmon waveguides. *Nat. Mater.* **2**, 229–232 (2003).
46. Tanaka, K. & Tanaka, M. Simulations of nanometric optical circuits based on surface plasmon polariton gap waveguide. *Appl. Phys. Lett.* **82**, 1158–1160 (2003).
47. Stockman, M. I. Nanofocusing of optical energy in tapered plasmonic waveguides. *Phys. Rev. Lett.* **93**, 137404 (2004).
48. Aubry, A. *et al.* Plasmonic Light-Harvesting Devices over the Whole Visible Spectrum. *Nano Lett.* **10**, 2574–2579 (2010).
49. Verhagen, E., Kuipers, L. & Polman, A. Plasmonic Nanofocusing in a Dielectric Wedge. *Nano Lett.* **10**, 3665–3669 (2010).
50. Gramotnev, D. K. & Vernon, K. C. Adiabatic nano-focusing of plasmons by sharp metallic wedges. *Appl. Phys. B-Lasers Opt.* **86**, 7–17 (2007).
51. Genet, C. & Ebbesen, T. W. Light in tiny holes. *Nature* **445**, 39–46 (2007).
52. Bethe, H. A. Theory of Diffraction by Small Holes. *Phys. Rev.* **66**, 163–182 (1944).
53. Chen, F. *et al.* Imaging of optical field confinement in ridge waveguides fabricated on very-small-aperture laser. *Appl. Phys. Lett.* **83**, 3245–3247 (2003).
54. Matteo, J. A. *et al.* Spectral analysis of strongly enhanced visible light transmission through single C-shaped nanoapertures. *Appl. Phys. Lett.* **85**, 648–650 (2004).
55. Rao, Z., Hesselink, L. & Harris, J. S. High transmission through ridge nano-apertures on vertical-cavity surface-emitting lasers. *Opt. Express* **15**, 10427–10438 (2007).
56. Wang, L., Uppuluri, S. M., Jin, E. X. & Xu, X. F. Nanolithography using high transmission nanoscale bowtie apertures. *Nano Lett.* **6**, 361–364 (2006).
57. Sakai, T., Nakano, I., Shimo, M., Takamori, N. & Takahashi, A. Thermal direct mastering using deep UV laser. *Jpn. J. Appl. Phys. Part 1 - Regul. Pap. Brief Commun. Rev. Pap.* **45**, 1407–1409 (2006).
58. Ito, E., Kawaguchi, Y., Tomiyama, M., Abe, S. & Ohno, E. TeOx-based film for heat-mode inorganic photoresist mastering. *Jpn. J. Appl. Phys. Part 1 - Regul. Pap. Short Notes Rev. Pap.* **44**, 3574–3577 (2005).
59. Juang, J. Y., Bogy, D. B. & Bhatia, C. S. Design and dynamics of flying height control slider with piezoelectric nanoactuator in hard disk drives. *J. Tribol.-Trans. ASME* **129**, 161–170 (2007).
60. Pan, L. & Bogy, D. B. Heat-assisted magnetic recording. *Nat. Photonics* **3**, 186–187 (2009).

Acknowledgments

This work is financially supported by NSF Nano-scale Science and Engineering Center (NSEC) for Scalable and Integrated Nanomanufacturing (SINAM) (Grant No.

CMMI-0751621) and in collaboration with Computer Mechanics Laboratory (CML) of University of California, Berkeley.

Author contributions

X.Z. guided the experiments and system development. L.P. and C.S. designed and developed the optical, thermal, and mechanical system. Y.X., L.P. and C.S. designed the plasmonic lenses. Y.P. and J.R. fabricated the plasmonic lenses and plasmonic flying heads. E.U., S.X. and L.Z. designed the high-speed lithography pattern generator. L.P., Y.W. and D.B.B. designed and tested air bearing surface and plasmonic flying heads. L.P. and Y.X. conducted experiments on plasmonic nanolithography. L.P., Y.P. and Y.X. contributed equally to this work.

Additional information

Supplementary information accompanies this paper at http://www.nature.com/scientificreports

Competing financial interests: The authors declare no competing financial interests.

How to cite this article: Pan, L. *et al*. Maskless Plasmonic Lithography at 22 nm Resolution. *Sci. Rep.* **1**, 175; DOI:10.1038/srep00175 (2011).